ISSN 1063-7834, Physics of the Solid State, 2016, Vol. 58, No. 7, pp. 1361–1370. © Pleiades Publishing, Ltd., 2016.
Original Russian Text © T.V. Drokina, G.A. Petrakovskii, M.S. Molokeev, V.S. Bondarev, D.A. Velikanov, 2016, published in Fizika Tverdogo Tela, 2016, Vol. 58, No. 7, pp. 1316–1324.

MAGNETISM

Synthesis and Study of Structural, Thermodynamic, and Magnetic Properties of $Na_xLi_{1-x}FeGe_2O_6$ ($x = 0.1–0.9$) Compounds

T. V. Drokina[a, *], G. A. Petrakovskii[a], M. S. Molokeev[a, b], V. S. Bondarev[a, c], and D. A. Velikanov[a, c]

[a] *Kirensky Institute of Physics, Siberian Branch of the Russian Academy of Sciences, Akademgorodok 50-38, Krasnoyarsk, 660036, Russia*

[b] *Far Eastern State Transport University, ul. Serysheva 47, Khabarovsk, 680000, Russia*

[c] *Siberian Federal University, pr. Svobodnyi 79, Krasnoyarsk, 660041, Russia*

**e-mail: tvd@iph.krasn.ru*

Received January 11, 2016

Abstract—The properties of $Na_xLi_{1-x}FeGe_2O_6$ ($x = 0.1–0.9$) solid solutions obtained via a solid-phase synthesis have been measured by X-ray diffraction, calorimetry, and magnetic method. The order–disorder transformations in low-dimensional $Na_xLi_{1-x}FeGe_2O_6$ ($x = 0.1–0.9$) spin systems with predominately antiferromagnetic exchange interaction have been revealed in the low-temperature susceptibility dependences. The study of thermal and physical properties has confirmed that substituting the sodium ions with the lithium ones induces the first-order structural phase transitions of the displacement type which are characterized by a symmetry change in monoclinic crystals from high-temperature $C2/c$ space group to low-temperature $P2_1/c$ space group.

DOI: 10.1134/S1063783416070143

1. INTRODUCTION

Pyroxenes are described by a general formula ABX_2O_6 (here, A is a mono- or bivalent metal cation [Na, Li, Ca]; B are tri- or bivalent metal cations [Mg, Cr, Cu, Ni, Co, Fe, Mn, Al, Ga, Ti, Sc, In, V...]; X are the [Ge, Si] cations) and form a wide class of compounds. Their crystal structure is characterized by isolated AO_6 (A = Fe, Ti, V, and Cr) octahedron chains along the crystal axis c. The magnetic interaction between them is weak because of the nonmagnetic $Ge(Si)O_4$-tetrahedron chains, which are also extended along c axis. These chains alternate along b crystal axis.

The magnetic properties of pyroxenes are known by their diversity [1—5] due to their specific crystal structure, which allows for low dimensionality of magnetic systems and competition exchange processes that raises interest of researchers in condensed matter physics. Studying pyroxenes is attractive not only in a fundamental point of view, but for practical applications. For example, $NaFeGe_2O_6$ clinopyroxene reveals the dependence of the electrical properties on the magnetic field [6].

Spinodal decay in artificial pyroxenes [7, 8] and lunar rock pyroxenes [9] is characterized by matter decomposition into different phases, being the initial stage of their phase transitions that is also of great attention of researches in both theoretical and practical aspects. The nontypical linear dependence of the luminescence spectrum in $Na_{1-x}Ca_xSc_{1-x}Mg_xSi_2O_6 : Eu^{2+}$ systems [10] became possible due to the nanosegregation of domains in $NaScSi_2O_6$ and $CaMgSi_2O_6$ compounds. In turn, nanosegregation is caused by various Na/Mg and Ca/Mg ions in A and B positions, respectively. Nevertheless, the effect of cation substitution on the phase states and transitions in pyroxenes is still poorly understood.

The temperature changes and cation substitutions at X and A positions in pyroxenes favor the structural phase transitions with the alteration in a monoclinic symmetry space group $C2/c \leftrightarrow P2_1/c$ [11—14]. The crystal symmetry of $Na_xLi_{1-x}FeGe_2O_6$ systems at room temperature is described by the monoclinic space groups $C2/c$ ($x = 1$) [15] and $P2_1/c$ ($x = 0, 0.5$) [12, 16]. The works [11, 13] report the study of structural transformations in $Na_xLi_{1-x}FeGe_2O_6$ pyroxene solid solutions via X-ray diffraction and nuclear gamma resonance. The structural properties are closely related to the magnetic properties of materials that results in the noticeable differences in the magnetic structures typical of $C2/c$ and $P2_1/c$ groups in clinopyroxenes [14, 17].

The aforementioned defines the topicality to study the magnetic properties and phase transitions in

Table 1. Basic parameters of experiment and establishment of $Na_xLi_{1-x}FeGe_2O_6$ structures

Parameter	$x = 0.1$	$x = 0.2$	$x = 0.5$	$x = 0.7$	$x = 0.9$
Space group	$P2_1/c$	$P2_1/c$	$C2/c$	$C2/c$	$C2/c$
a, Å	9.9048(1)	9.9253(2)	10.0333(1)	10.0175(1)	10.0110(1)
b, Å	8.8251(1)	8.8354(1)	8.8136(1)	8.8636(1)	8.90170(8)
c, Å	5.4010(1)	5.4226(1)	5.52965(9)	5.52420(8)	5.51505(6)
β, deg	108.7956(9)	108.7299(9)	108.921(1)	108.3989(8)	107.8227(7)
V, Å^3	446.93(1)	450.35(1)	426.56(1)	456.43(1)	467.887(9)
Z	4	4	4	4	4
Range 2θ, deg	5–140	5–140	5–120	5–110	5–110
R_{wp}, %	2.79	2.69	3.59	3.39	2.96
R_p, %	2.12	2.03	2.67	2.67	2.33
R_{exp}, %	2.02	1.87	2.14	2.78	2.59
χ^2	1.38	1.44	1.68	1.22	1.14
R_B, %	1.49	1.24	1.85	1.55	1.37

a, b, c, β are the lattice parameters; V is the lattice volume; Z is the number of formula unit; the unreability factors: R_B is the integral, R_{wp} is the weight profile, R_p is the profile, R_{exp} is the expected; $\chi^2 = R_{wp}/R_{exp}$ is the quality of fitting.

$Na_xLi_{1-x}FeGe_2O_6$ pyroxenes ($x = 0.1$–0.9). The present work is thus aimed at characterizing the effect of substitution of the sodium ions with lithium ones on the magnetic and heat properties of $Na_xLi_{1-x}FeGe_2O_6$ solid solutions.

2. SYNTHESIS OF SAMPLES AND EXPERIMENTAL TECHNIQUE

$Na_xLi_{1-x}FeGe_2O_6$ ($x = 0.1$–0.9) samples were prepared via a solid-phase chemical reaction from a blend of Fe_2O_3, Na_2CO_3, Li_2CO_3, and GeO_2 oxides with respect to the compound stoichiometry. The samples were molded under pressure in the pellets with a diameter of 10 mm and a thickness of 1.5–2.0 mm and then subjected to three-stage annealing at temperatures of 800–1000°C in air with the intermediate wet milling in an alcohol medium and subsequent remolding. The chemical and phase composition of samples was controlled via X-ray diffraction. The powder X-ray profiles of $Na_xLi_{1-x}FeGe_2O_6$ ($x = 0.1, 0.2, 0.5, 0.7, 0.9$) were recorded on a D8 ADVANCE Bruker diffractometer with using a VANTEC linear detector and CuK_α radiation at the increment of 0.016° and increment exposure of 2.7 s.

The heat and physical studies of $Na_xLi_{1-x}FeGe_2O_6$ systems were carried out on a DSM-10ma differential scanning microcalorimeter in the temperature range of 100–730 K. The ceramic samples used earlier for establishing the structure were triturated in an agate mortar to achieve ultradispersed powder and packed under press in an aluminum container. The heat capacity was measured in a helium atmosphere on ~60 mg samples in the dynamic mode with the rate of temperature change of $dT/d\tau = 8$–16 K min^{-1}. The deviation of the experimental points from the smoothed curve $C_p(T)$ was below 1%. The error in measuring the integral characteristics (enthalpy and entropy) was ~10–20% depending on the heat effect value.

The static magnetic characteristics of samples were measured on a SQUID magnetometer at the Institute of Physics (Siberian Branch of the Russian Academy of Sciences) within the temperature range of 4–300 K in the magnetic field of $H = 500$ Oe.

3. RESULTS

The structural properties of the polycrystalline $Na_xLi_{1-x}FeGe_2O_6$ compounds ($x = 0.1, 0.2, 0.5, 0.7$, and 0.9) were studied via X-ray diffraction. The difference X-ray profiles are shown in Fig. 1. The X-ray diffractions of compounds with the concentration $x =$ [0.1, 0.2] are attributed to a monoclinic $P2_1/c$ cell with the parameters close to $LiFeGe_2O_6$ system [14], whereas the reflections in the X-ray diffractograms of samples with $x =$ [0.5 [12], 0.7, 0.9] are indicated by another space group $C2/c$ group with the parameters close to $NaFeGe_2O_6$ [13, 14]. In comparison with the $C2/c$ phase, a $P2_1/c$ phase has the weak superstructure (hkl) reflections at $h + k = 2n + 1$ that was used as a criterion of the any phase formation (Fig. 1). The atomic coordinates of $NaFeGe_2O_6$ and $LiFeGe_2O_6$ phases were used to establish the structure of the studied compounds by the Rietveld method. The Na and Li atoms were at the Na positions in the context of this model.

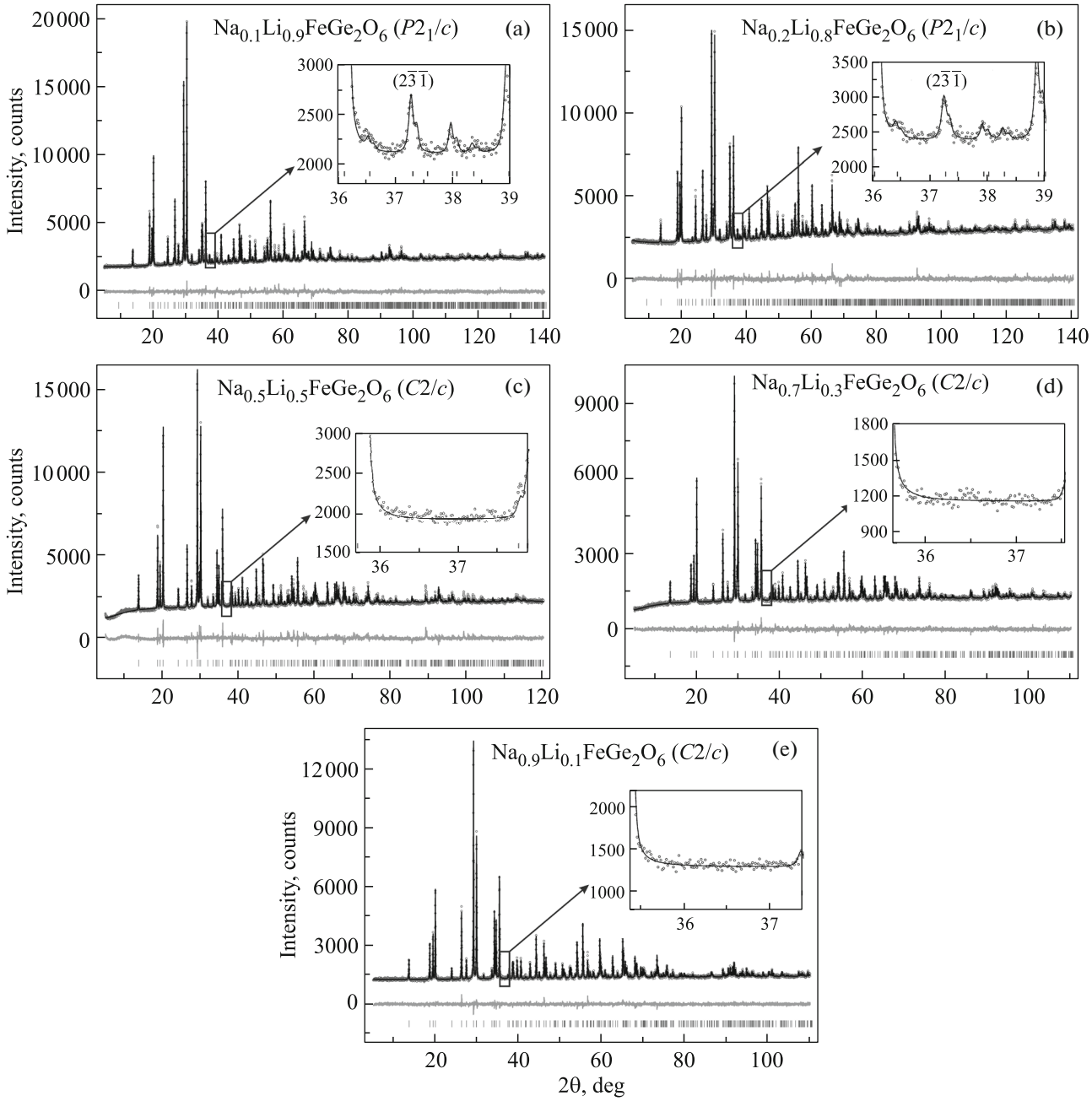

Fig. 1. Room-temperature difference X-ray profiles of $Na_xLi_{1-x}FeGe_2O_6$ compound. x = (a) 0.1, (b) 0.2, (c) 0.5, (d) 0.7, and (e) 0.9. The insert shows a $(2\bar{3}\bar{1})$ superstructure peak allowed in $P2_1/c$ and forbidden in $C2/c$ group.

Population of their positions was fixed in accordance with the assumed chemical formula. The establishment was implemented in the TOPAS 4.2 software [18] and gave the low R-factors (Fig. 1, Table 1). The general structure of these compounds is displayed in Fig. 2. The atomic coordinates are shown in Table 2.

According to the X-ray studies, the unit cell volume as a function of the sodium concentration x for each of two phases with using the data [14, 19] is linear in coincidence with the Vegard's law. Herewith, at $x \sim 0.5$ there is an abrupt increase in the volume $\Delta V \sim 5$ Å^3 (Fig. 3a) that is due to the fact that $P2_1/c \leftrightarrow C2/c$ is a first-order phase transition. The linear segments of the volume as a function of the sodium content confirm the assumed concentrations x of the studied compounds are close to the real values. We note that the results obtained on polycrystalline compounds coincide with the experimental data on single crystals [13]. In our case, we had large-volume powder samples with a good quality to study the physical properties.

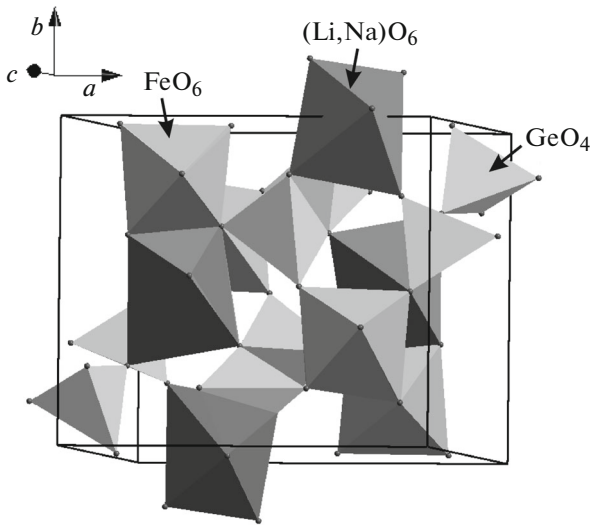

Fig. 2. $Na_xLi_{1-x}FeGe_2O_6$ structure. The Li and Na ions hold the same position.

It is worth mentioning that the changes in the bind length and valence angles as depending on x concentration were analyzed in detail in [13]. This allowed one to determine in combination with Mössbauer spectroscopy that the intermediate compounds with the values x around 0.5 have the most distorted $(Li,Na)O_6$ octahedra. In contrast, the systems with $x = [0, 1]$ are characterized by the least distorted octahedra, and distortion in a $C2/c$ phase ($x = 1$) is less than in a $P2_1/c$ phase ($x = 0$). We think this result can be obtained the most completely and easily in the numerical values by calculating the index of octahedron distortion using the formula $D = (1/n)\Sigma((L_i - \langle L\rangle)/\langle L\rangle)$ [20], where L_i is the distance from the central atom of polyhedron to i-st coordinating atom, $\langle L\rangle$ is the average bind length.

Figure 3b displays the distortion index for our experimental data and those from [13]. The qualitative agreement is evident not only between the data in both works, but also when the distortion of a $(Li,Na)O_6$ polyhedron is assumed to increase upon alloying of the $LiFeGe_2O_6$ and $NaFeGe_2O_6$ compounds with the Na and Li ions until the phase transition at $x \approx 0.5$.

In order to detect the possible phase structural transformations typical of the chain pyroxenes and to determine the basic parameters characterizing the heat properties, we have studied the heat and physical properties of $Na_xLi_{1-x}FeGe_2O_6$ solid solutions (x = 0.1, 0.2, 0.5, 0.51, 0.7, and 0.9). Figure 4 shows the temperature dependence of the excess heat capacity for $Na_xLi_{1-x}FeGe_2O_6$ systems, which is evaluated by extraction of the lattice component C_{lat} from the total heat capacity. The $C_{lat}(T)$ dependence was approximated by a smooth polynomial function matching the

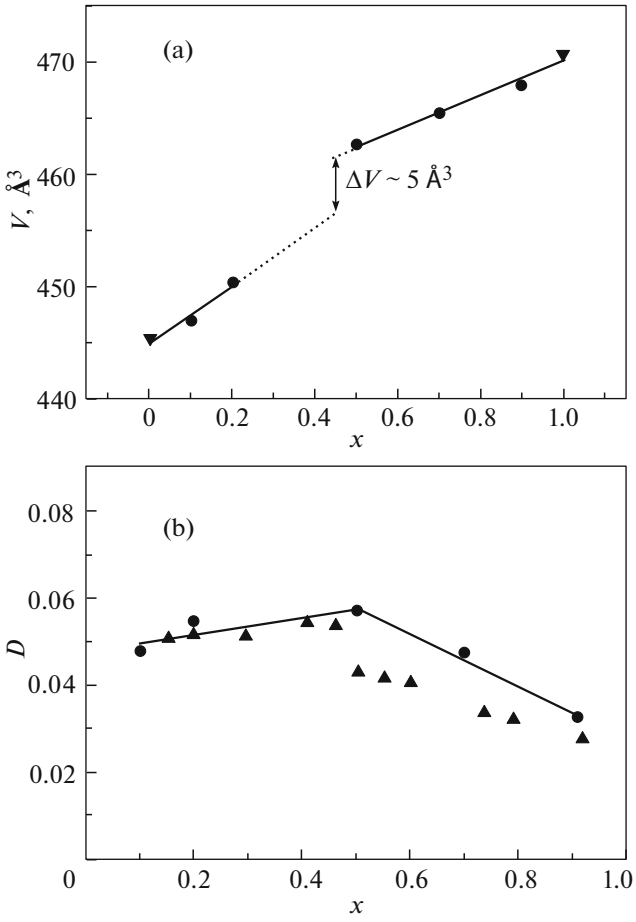

Fig. 3. (a) Linear dependence of the unit cell volume on x concentration at $T = 300$ K. Circles are the data for the studied compounds, triangles are the parameters from [14, 19]. (b) Distortion index D of $(Li,Na)O_6$ polyhedron, calculated for compounds used in this work (circles) and in [13] (triangles). The distortion index increases at doping the $LiFeGe_2O_6$ and $NaFeGe_2O_6$ systems with the Na and Li ions until the phase transition at $x \approx 0.5$.

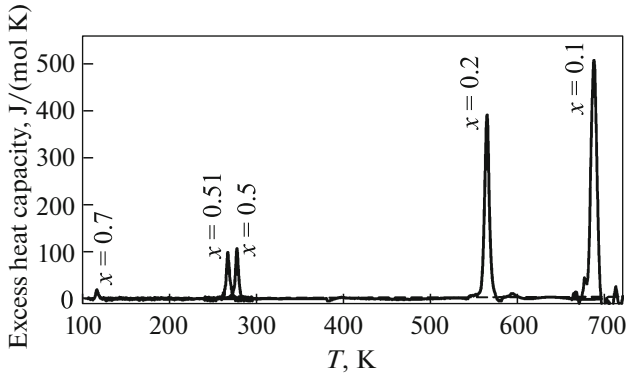

Fig. 4. Excess heat capacity as a function of temperature for $Na_xLi_{1-x}FeGe_2O_6$ solid solutions.

Table 2. Atomic coordinates and parameters of $Na_xLi_{1-x}FeGe_2O_6$ compounds

Atom	x	y	z	B_{iso}	Population of the position
			$Na_{0.1}Li_{0.9}FeGe_2O_6$		
Fe	0.2524(8)	0.6491(4)	0.234(2)	0.3(1)	1
Li	0.262(5)	0.013(3)	0.19(1)	0.5(8)	0.9
Na	0.262(5)	0.013(3)	0.19(1)	0.5(8)	0.1
Ge1	0.0428(4)	0.3416(6)	0.2855(9)	0.3(1)	1
Ge2	0.5529(4)	0.8405(6)	0.2338(9)	0.3(1)	1
O1	0.860(2)	0.351(2)	0.202(4)	0.5(2)	1
O2	0.114(2)	0.514(2)	0.287(4)	0.5(2)	1
O3	0.096(2)	0.264(2)	0.585(5)	0.5(2)	1
O4	0.360(2)	0.817(2)	0.146(5)	0.5(2)	1
O5	0.624(2)	1.010(2)	0.386(4)	0.5(2)	1
O6	0.607(2)	0.674(1)	0.448(4)	0.5(2)	1
			$Na_{0.2}Li_{0.8}FeGe_2O_6$		
Fe	0.2537(9)	0.6494(5)	0.216(1)	0.3(1)	1
Li	0.255(6)	0.023(3)	0.22(1)	0.5(6)	0.8
Na	0.255(6)	0.023(3)	0.22(1)	0.5(6)	0.2
Ge1	0.0461(5)	0.3460(5)	0.272(1)	0.3(1)	1
Ge2	0.5483(5)	0.8388(6)	0.234(1)	0.3(1)	1
O1	0.859(3)	0.329(3)	0.163(5)	0.5(2)	1
O2	0.110(3)	0.520(2)	0.308(4)	0.5(2)	1
O3	0.120(2)	0.272(2)	0.594(6)	0.5(2)	1
O4	0.358(2)	0.834(3)	0.119(5)	0.5(2)	1
O5	0.624(2)	1.004(3)	0.383(5)	0.5(2)	1
O6	0.598(2)	0.695(2)	0.501(5)	0.5(2)	1
			$Na_{0.5}Li_{0.5}FeGe_2O_6$		
Li	0	0.292(2)	0.25	0.5(4)	0.5
Na	0	0.292(2)	0.25	0.5(4)	0.5
Fe	0	0.9063(5)	0.25	0.5(2)	1
Ge	0.2878(2)	0.0920(3)	0.2381(5)	0.5(2)	1
O1	0.1009(8)	0.091(1)	0.163(2)	1.0(3)	1
O2	0.360(1)	0.274(1)	0.308(2)	1.0(3)	1
O3	0.343(1)	0.003(1)	0.033(4)	1.0(3)	1
			$Na_{0.7}Li_{0.3}FeGe_2O_6$		
Na	0	0.281(1)	0.25	2.7(4)	0.7
Li	0	0.281(1)	0.25	2.7(4)	0.3
Fe	0	0.9018(5)	0.25	0.6(2)	1
Ge	0.2898(2)	0.0943(2)	0.2363(4)	0.5(2)	1
O1	0.1050(8)	0.076(1)	0.149(2)	1.0(2)	1
O2	0.356(1)	0.278(1)	0.306(2)	1.0(2)	1
O3	0.355(1)	0.0117(9)	0.032(3)	1.0(2)	1
			$Na_{0.9}Li_{0.1}FeGe_2O_6$		
Na	0	0.290(1)	0.25	2.4(3)	0.9
Li	0	0.290(1)	0.25	2.4(3)	0.1
Fe	0	0.9020(4)	0.25	0.6(2)	1
Ge	0.2889(2)	0.0938(2)	0.2312(3)	0.5(2)	1
O1	0.1041(6)	0.0803(9)	0.138(2)	1.0(2)	1
O2	0.3584(8)	0.2710(9)	0.298(2)	1.0(2)	1
O3	0.3590(9)	0.0030(7)	0.024(2)	1.0(2)	1

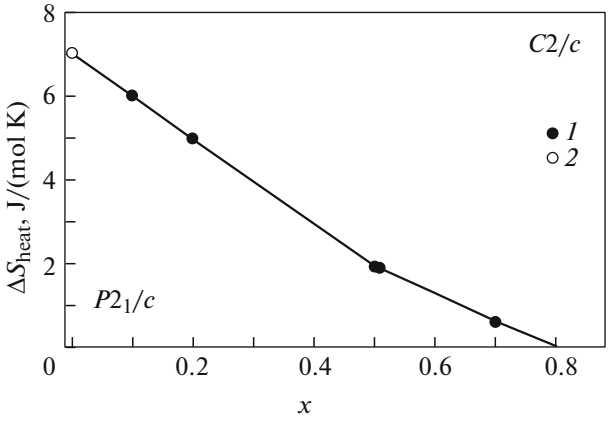

Fig. 5. ΔS–x phase diagram of $Na_xLi_{1-x}FeGe_2O_6$ solid solutions. *1*—experimental results, *2*—calculated data.

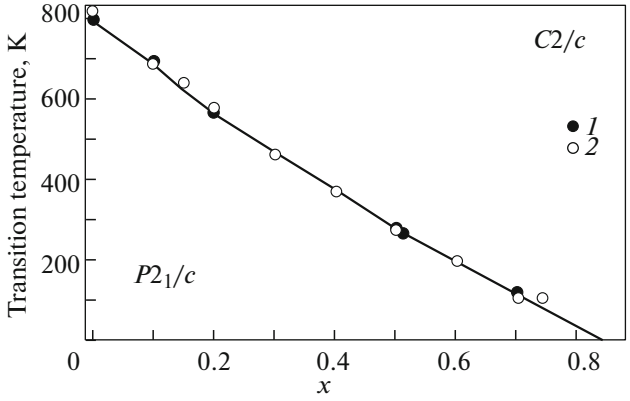

Fig. 6. T–x phase diagram of $Na_xLi_{1-x}FeGe_2O_6$ systems. *1*—results in the present work, *2*—experimental data from [13, 16].

experimental curve beyond the anomaly heat capacity range.

The solid solution with the sodium concentration $x = 0.1$ at $T = 687$ K exhibits the first-order structural phase transition ($P2_1/c \rightarrow C2/c$) with the temperature hysteresis $\delta T = 20$K. Integrating the function $(\Delta C_p/T)(T)$ over the studied temperature range enabled us to establish a total change in enthalpy $\Delta S = 6.0 \pm 0.6$ J/(mol K) due to the observed phase transformation. This value ΔS is typical of the displacement phase transitions and does not correspond to the ordering in the considered solid solution. As is shown, increasing the Na concentration (x = 0.2, 0.5, 0.51, and 0.7) favors a decrease in the heat capacity anomaly and its shift towards low temperatures. The integral thermodynamic characteristics (a change in entropy ΔS and enthalpy ΔH) for $Na_xLi_{1-x}FeGe_2O_6$ solid solutions are presented in Table 3 in the heat and cool modes. We note that at $x = 0.9$, no specific heat capacity behavior was found in the studied temperature range.

Figure 5 displays the ΔS–x phase diagram of $Na_xLi_{1-x}FeGe_2O_6$ solid solutions. Obviously, the phase boundary at the sodium content from $x = 0.1$ to x = 0.5 is described by the linear dependence in the limits of the error. It can thus assume that at $x = 0$ the changes in entropy and enthalpy after the phase transition will be $\Delta S \sim 7$ J/(mol K) and $\Delta H \sim 5530$ J/mol. In this case the phase transition for $LiFeGe_2O_6$ compound is implemented at $T \approx 790$ K.

Earlier, the $P2_1/c \leftrightarrow C2/c$ phase transformation in $LiFeGe_2O_6$ was experimentally studied in [14]. It was shown to occur at $T = 789$ K, which is in agreement with the above-estimated phase transition point.

The linear dependence retains itself at increasing the sodium concentration $x > 0.5$, but there is a change in the angle of the straight inclination. A range nearby $x = 0.5$ corresponds to the phase boundary fracture and reveals an abrupt increase in the volume of $\Delta V \sim 5$ Å^3 (Fig. 3a) that is assumed to be due to slight positional (Li,Na) disordering in the octahedron at A position [13]. With a further increase in the sodium concentration x, the coexistence range of the $P2_1/c$ phase decreases with the emergence of only the $C2/c$ phase at $x > 0.8$. The last one is retained until the lowest temperatures accessible during the experiment.

Based on our study and data from [13, 16], we have constructed the T–x phase diagram (Fig. 6) which

Table 3. Thermodynamic parameters of $Na_xLi_{1-x}FeGe_2O_6$ solid solutions

Parameter	$x = 0.1$	$x = 0.2$	$x = 0.5$	$x = 0.51$	$x = 0.7$
T_{heat}, K	686.9	564.2	276.4	265.9	115.4
T_{cool}, K	666.3	547.3	271.6	262.9	113.0
δT, K	20.6	16.9	4.8	3.0	2.6
ΔS_{heat}, J/(mol K)	6.0	5.0	1.92	1.88	0.6
ΔS_{cool}, J/(mol K)	6.6	6.1	1.98	1.7	0.7
ΔH_{heat}, J/mol	4150	2750	530	500	69
ΔH_{cool}, J/mol	4450	3350	536	440	79

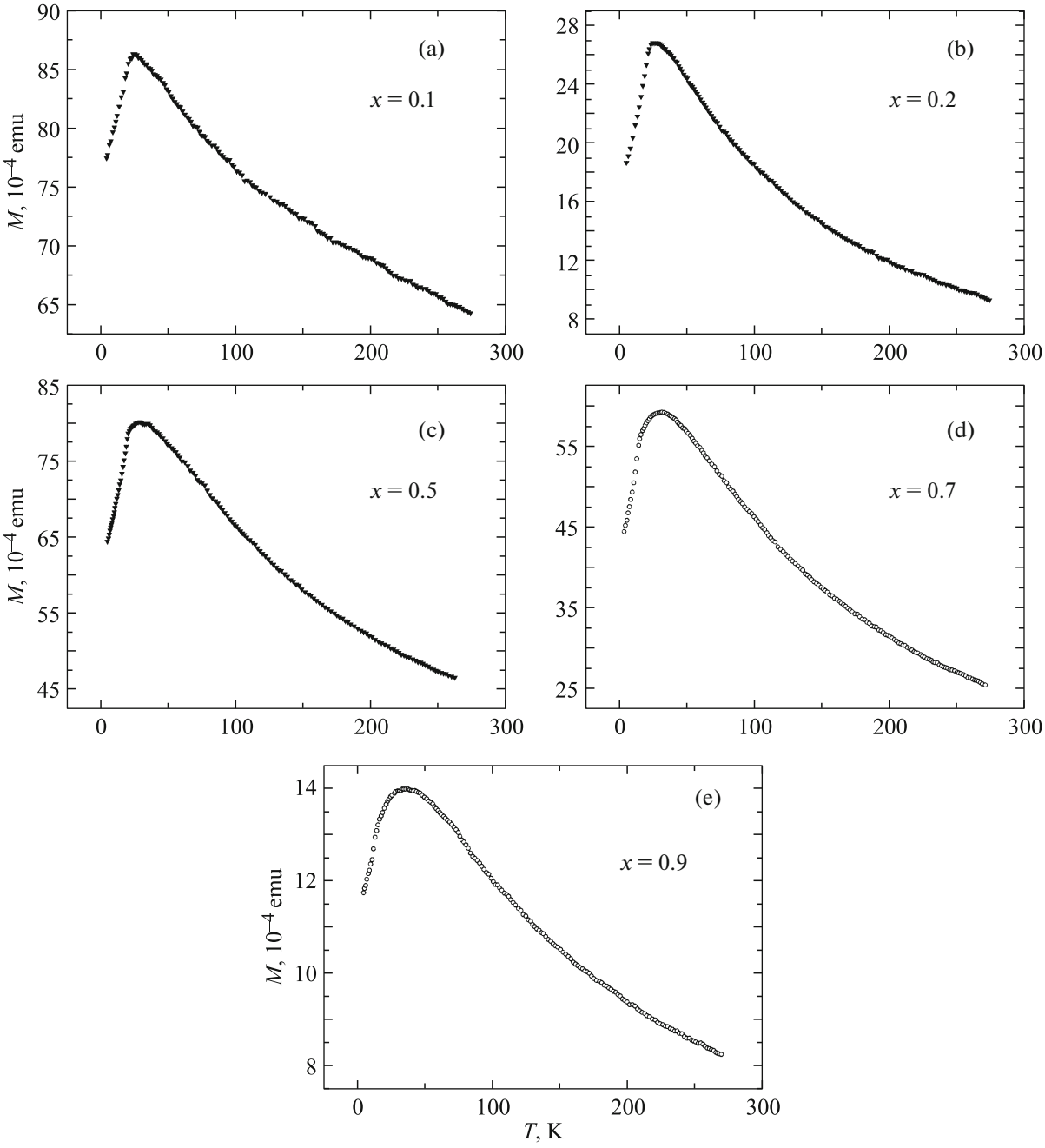

Fig. 7. Temperature dependences of the magnetic moment in $Na_xLi_{1-x}FeGe_2O_6$ compounds, measured in the magnetic field $H = 0.05$ T. $x =$ (a) 0.1, (b) 0.2, (c) 0.5, (d) 0.7, and (e) 0.9.

demonstrates a good agreement between the thermophysical and structural data on polycrystalline and single crystal samples.

Figures 7 and 8 and Table 4 show the magnetic measurement results for $Na_xLi_{1-x}FeGe_2O_6$ solid solutions ($x = 0.1$, 0.2, 0.5, 0.7, and 0.9; the sample weight is $m = 0.040$, 0.050, 0.125, 0.145, and 0.030 g, respectively) in the temperature range of 4–300 K. Figure 7 displays the temperature dependences of the magnetic moment M for $Na_xLi_{1-x}FeGe_2O_6$ compounds, measured in the magnetic field of 0.05 T. The curves characterizing the magnetic properties have the profiles typical of antiferromagnetics. The temperature dependences of the magnetic moment (Fig. 7) show the broad maxima at T_{max} (Table 4). The specific behavior of the $M(T)$ dependence with increasing temperature in $Na_xLi_{1-x}FeGe_2O_6$ allow interpretation of the maximum in the temperature dependence of the magnetic

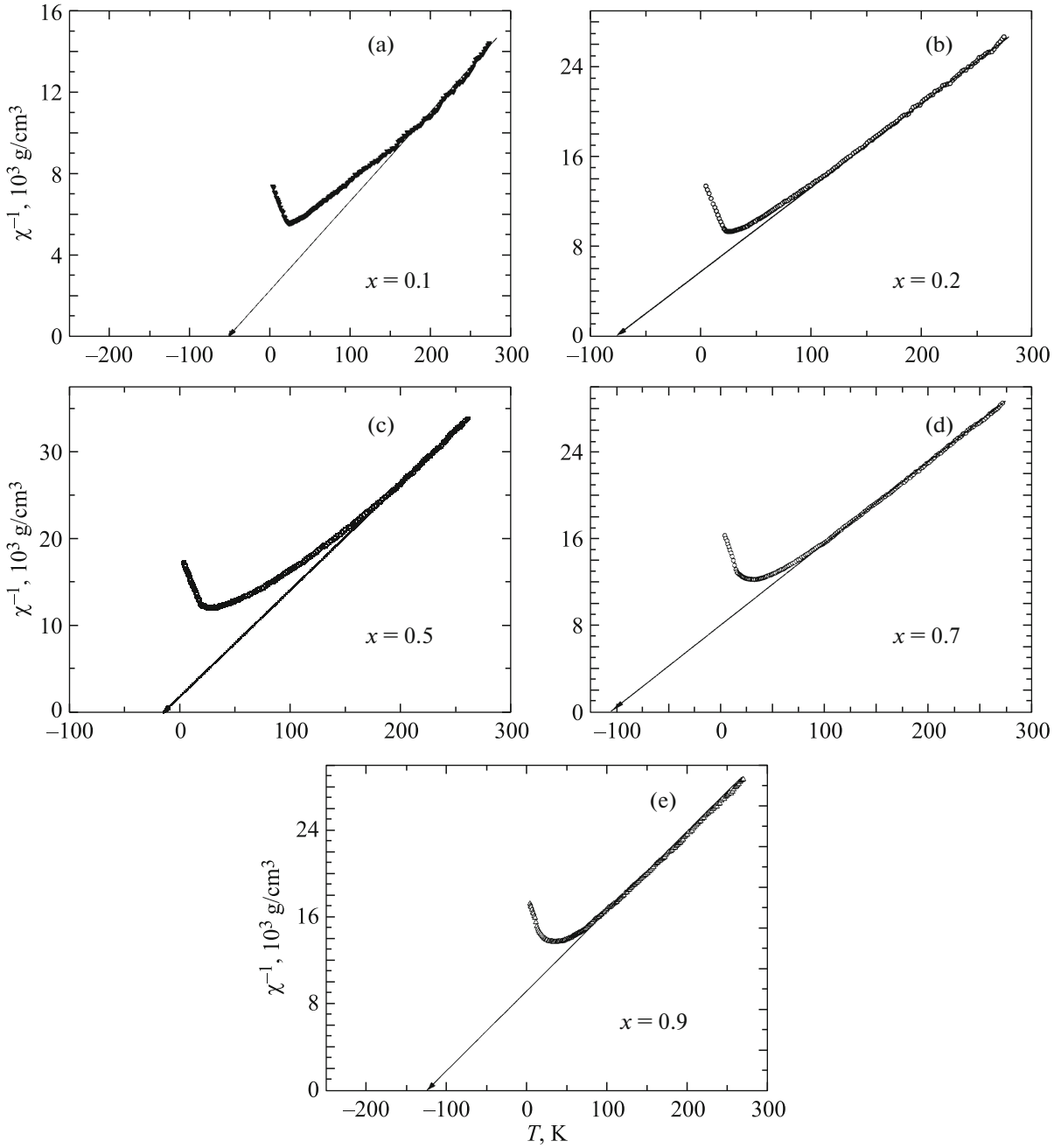

Fig. 8. Temperature dependences of the reverse susceptibility of $Na_xLi_{1-x}FeGe_2O_6$ systems, measured in the magnetic field H = 0.05 T. x = (a) 0.1, (b) 0.2, (c) 0.5, (d) 0.7, and (e) 0.9.

moment as the magnetic order–disorder phase transition. The Néel temperatures T_N defined as the maximum of the dM/dT derivative are shown in Table 4. We mention that $T_N/T_{max} < 1$ for all chain pyroxenes studied in this work.

Figure 8 displays the temperature dependence of the reverse magnetic susceptibility $\chi^{-1}(T)$ over the temperature range of 4—300 K for $Na_xLi_{1-x}FeGe_2O_6$ solid solutions (x = 0.1, 0.2, 0.5, 0.7, and 0.9). The behavior of the $\chi^{-1}(T)$ curves at high temperatures ($T > 100$–150 K) can be described by the Curie–Weiss law. We note that for samples with $x = 0.1$, 0.5, and 0.9 the constant component was taken into account in the Curie–Weiss law, which was evaluated experimentally. Its emergence is caused by the iron-containing impurity which was not detected via X-ray diffraction. The asymptotic Néel temperatures defined as the intersection points of the T temperature axis with the asymptote to the $\chi^{-1}(T)$ curve at high temperatures are nega-

Table 4. Néel temperature of magnetic ordering T_N, temperatures of maximum T_{max} in the temperature dependence of the magnetic moment, asymptotic Néel temperature Θ and effective moment for $Na_xLi_{1-x}FeGe_2O_6$ compounds ($x = 0.1–1$)

Compound	T_N, K	T_{max}, K	Θ, K	μ_{eff}, μ_B (experiment)
$NaFeGe_2O_6$	13	25	−135	5.89
$Na_{0.9}Li_{0.1}FeGe_2O_6$	11.9	35	−125	5.9
$Na_{0.7}Li_{0.3}FeGe_2O_6$	13.1	31	−107	5.8
$Na_{0.5}Li_{0.5}FeGe_2O_6$	18	27.5	−14	4.5
$Na_{0.2}Li_{0.8}FeGe_2O_6$	19	25	−75	5.7
$Na_{0.1}Li_{0.9}FeGe_2O_6$	17.8	24.5	−50	6.9

tive (Table 4). When decreasing the temperature below the Néel point, the $Na_xLi_{1-x}FeGe_2O_6$ samples ($x = 0.1–0.9$) are subjected to the transition from paramagnetic to the long-range magnetic state which is formed predominately by antiferromagnetic exchange interaction between the Fe^{3+} ions. The effective magnetic moment (molar values) determined experimentally (Table 4) are comparable with the calculated effective magnetic moment which is $\mu_{eff(calc)}^{Fe^{3+}} = 5.91\ \mu_B$.

The magnetic structure formation in pyroxenes is due to the complex competition of the exchange interactions between the nearest atomic neighbors and those subsequent. The spin structures are known for some of the magnetically ordered crystals. In the incommensurate magnetic structure $NaFeGe_2O_6$ with the $C2/c$ crystal symmetry up to 1.6K, the magnetic moments of the iron ions form the antiferromagnetically coupled pairs with helicoidal spin modulation along the propagation vector **k** (**k** = (0.3357(4), 0, 0.0814(3)) at $T = 1.6$ K) [4, 17]. In $Na_xLi_{1-x}FeGe_2O_6$ compounds ($x = 0$ and 0.5) with the crystal symmetry $P2_1/c$ in the coexistence long magnetic order there is the commensurate antiferromagnetic structure [1, 12]. It is characterized by the space group P_a2_1/c and double unit cell along the crystallographic axis a (for the sodium concentrations $x = 0.5$ the propagation vector is **k** = (1/2, 0, 0) at $T = 1.5$ K). The further study of solid solutions will be dedicated to the investigation of the $Na_xLi_{1-x}FeGe_2O_6$ magnetic structure, in order to detect the phase transformation of the modulated structure into a commensurate antiferromagnetic one.

4. CONCLUSIONS

The X-ray diffraction, calorimetry, and magnetic measurements allowed for study of magnetic and heat properties of $Na_xLi_{1-x}FeGe_2O_6$ solid solutions. These systems revealed the magnetic phase transitions from high-temperature paramagnetic state to low-temperature magnetically ordered state at low temperatures. The paramagnetic state at temperatures above $T = 100–150$ K are described by the Curie–Weiss law and are characterized by negative asymptotic Néel points that testifies to predominately antiferromagnetic exchange interaction in the spin system of $Na_xLi_{1-x}FeGe_2O_6$ compounds ($x = 0.1–0.9$).

The study of thermal and physical parameters of $Na_xLi_{1-x}FeGe_2O_6$ solid solution at temperatures of 100 to 730 K confirmed the presence of structural displacement phase transitions at $x < 0.9$ due to a change in the crystal symmetry from the space group $C2/c$ to the space group $P2_1/c$. The phase $T–x$ diagram enabled us to determine the coexistence region of $P2_1/c$ phase depending on the solid solution composition. The entropy and enthalpy changes were evaluated due to the structural phase transitions in $Na_xLi_{1-x}FeGe_2O_6$ systems ($x = 0.1–0.9$).

REFERENCES

1. G. J. Redhammer, G. Roth, W. Treutmann, M. Hoelzel, W. Paulus, G. Andre, C. Pietzonka, and G. Amthauer, J. Solid State Chem. **182**, 2374 (2009).
2. A. N. Vasiliev, O. L. Ignatchik, A. N. Sokolov, Z. Hiroi, M. Isobe, and Y. Ueda, Phys. Rev. B: Condens. Matter **72**, 012412 (2005).
3. G. Nenert, C. Ritter, M. Isobe, O. Isnard, A. N. Vasiliev, and Y. Ueda, Phys. Rev. B: Condens. Matter **80**, 024402 (2009).
4. T. Drokina, G. Petrakovskii, L. Keller, and J. Schefer, J. Phys.: Conf. Ser. **251**, 012016 (2010).
5. M. Isobe, E. Ninomiya, A. N. Vasiliev, and Y. Ueda, J. Phys. Soc. Jpn. **71**, 1423 (2002).
6. I. Kim, B.-G. Jeon, D. Patil, S. Patil, G. Nénert, and K. H. Kim, J. Phys.: Condens. Matter **24**, 306001 (2012).
7. C. M. Jantzen, Am. Mineral. **69**, 277 (1984).
8. M. A. Carpenter, Contrib. Mineral. Petrol. **71**, 289 (1980).
9. P. E. Champness and G. W. Lorimer, Contrib. Mineral. Petrol. **33**, 171 (1971).
10. Z. Xia, Yu. Zhang, M. S. Molokeev, V. V. Atuchin, and Y. Luo, Sci. Rep. **3**, 3310 (2013).
11. G. V. Novikov, L. V. Sipavina, and V. V. Fed'kin, Bull. Russ. Acad. Sci.: Phys. **71** (9), 1305 (2007).
12. T. V. Drokina, G. A. Petrakovskii, M. S. Molokeev, S. V. Misyul, V. S. Bondarev, D. A. Velikanov, M. Frontzek, and J. Schefer, J. Magn. Magn. Mater. **385**, 243 (2015).

13. G. J. Redhammer and G. Tippelt, Phys. Chem. Miner. **43**, 1 (2016).
14. G. J. Redhammer, F. Camara, M. Alvaro, F. Nestola, G. Tippelt, S. Prinz, J. Simons, G. Roth, and G. Amthauer, Phys. Chem. Miner. **37**, 685 (2010).
15. L. P. Solov'eva and V. V. Bakakin, Sov. Phys. Crystallogr. **12**, 517 (1967).
16. M. Behruzi, Th. Hahn, C. T. Prewitt, and K. Baldwin, Acta Crystallogr., Sect. A: Found. Crystallogr. **40** (Suppl.), C247 (1984).
17. T. V. Drokina, G. A. Petrakovskii, L. Keller, J. Schefer, A. D. Balaev, A. V. Kartashev, and D. A. Ivanov, J. Exp. Theor. Phys. **112** (1), 121 (2011).
18. *Bruker AXS TOPAS V4: General Profile and Structure Analysis Software for Powder Diffraction Data. User's Manual* (Bruker AXS, Karlsruhe, Germany, 2008).
19. G. J. Redhammer, A. Senyshyn, M. Meven, G. Roth, S. Prinz, A. Pachler, G. Tippelt, C. Pietzonka, W. Treutmann, M. Hoelzel, B. Pedersen, and G. Amthauer, Phys. Chem. Miner. **38**, 139 (2011).
20. W. H. Baur, Acta Crystallogr., Sect. B: Struct. Crystallogr. Cryst. Chem. **30**, 1195 (1974).

Translated by O. Maslova